Multisensory integration (MSI) by polymodal sensory neurons dictates larval settlement in a brainless cnidarian larva

Sydney Birch*[1,2], David Plachetzki[1]

[1]Department of Molecular, Cellular, and Biomedical Sciences; University of New Hampshire; Durham, NH, 03824; USA

[2]Department of Biological Sciences; University of North Carolina Charlotte; Charlotte, NC, 28223; USA

Corresponding authors:
sbirch1@uncc.edu

Summary

Multisensory integration (MSI) combines information from more than one sensory modality to elicit behaviors distinct from unisensory behaviors. MSI is best understood in animals with complex brains and specialized centers for parsing sensory information, but the dispersive larvae of sessile marine invertebrates utilize multimodal environmental sensory stimuli to base irreversible settlement decisions on, and most lack complex brains. Here, we examined the sensory determinants of settlement in actinula larvae of the hydrozoan *Ectopleura crocea* (Cnidaria), which possess a diffuse nerve net. A factorial settlement study revealed that photo-, chemo-, and mechano-sensory cues each influence the settlement response, which was complex and dependent on specific combinations of cues, therefore indicating MSI. Mechanosensory cues either inhibited or enhanced settlement rates depending on the presence or absence of chemical and light cues in the environment. Sensory gene expression over development peaked with developmental competence to settle, which in actinulae, requires cnidocyte discharge. Transcriptome analyses also highlighted several deep homological links between cnidarian and bilaterian mechano- chemo- and photo-sensory pathways. Fluorescent *in situ* hybridization studies of candidate transcripts suggested cellular partitioning of sensory function among the few cell types that comprise the actinula nervous system, where ubiquitous polymodal sensory neurons with putative chemo- and photo-sensitivity interface with mechanoreceptive cnidocytes. We propose that a simple multisensory processing circuit, involving polymodal chemo/photosensory neurons and mechanoreceptive cnidocytes, is sufficient to explain MSI in actinulae settlement. Our study demonstrates that MSI is not exclusive to complex brains, but likely predated and contextualized their evolution.

Introduction

A distinguishing feature of animals is their exquisite capacity to receive sensory information from the environment and integrate it into behavior. Animals may integrate sensory signals from individual modalities (e.g. vision or taste), or they may perform multisensory integration (MSI), which combines information from more than one modality to elicit behaviors that are distinct from those elicited by unisensory behaviors (Stein et al. 1989, 2009, 2014; Stein and Meredith 1993; Alvarado et al. 2007; Otto et al. 2013; Stevenson et al. 2014).

MSI is best understood in bilaterian animals with complex nervous systems that include specialized centers for information processing and exchange (Stein 1998; Otto et al. 2013; Stein et al. 2014; Ghosh et al. 2017; Currier and Nagel 2020). Classically, MSI studies are conducted at the neuron level where neuronal signals are processed in the brain to make behavioral decisions (Meredith and Stein 1983; Stein 1998; Stein and Stanford 2008; Otto et al. 2013). However, much less research has been conducted on organisms without complex nervous systems or brains. Moreover, it has been shown that zoospores of an *Allomyces* fungus utilize a multisensory system involving chemo- and photo-taxis (Swafford and Oakley 2018) which suggests the possibility that MSI evolved prior to the evolution of complex nervous systems.

Sensory integration is critically important for sessile marine invertebrates that utilize larvae for dispersal and often make irreversible settlement decisions. Because some sensory cues may be better indicators of site quality than others, it has been proposed that larvae place emphasis on select cues, leading to a hierarchy of sensory cues that determine where settlement occurs (Kingsford et al. 2002; Müller and Leitz 2002; Woodson et al. 2007; Hodin et al. 2018). However, MSI has yet to be demonstrated in marine invertebrate larval settlement, and little is known about the potential for MSI in such organisms that lack complex nervous systems or brains.

The marine hydrozoan *Ectopleura crocea* is a benthic colonial species with a pan-global distribution in temperate coastal regions. Unlike many other cnidarians, *E. crocea* possesses an actinula larva (Fig 1C). Actinulae are motile lecithotrophic larvae that develop in the following five stages: the star embryo, preactinula, actinula, nematocyte-printing (settling) actinula, and settled actinula. *E. crocea* actinulae larvae begin settlement using a larval behavior called nematocyte-printing, which serves to tether actinula to the substrate (Yamashita 2003). However, little is known about the sensory cues that determine this process, the cell types that receive such information, or the underlying genetic machinery of sensation that coordinates such settlement decisions.

Here we describe integrative studies on the sensory biology of settlement in the actinulae of *Ectopleura crocea*. Immunohistochemical studies of larval neural network development indicate that *E. crocea* larvae first possess a defined nervous system complete with robust tentacular cnidocytes and sensory neurons by the actinula stage of development. Next, to identify the sensory cues involved in settlement, we performed a factorial larval settlement study that investigated the effects of individual and combined cues (e.g., light, chemical (biofilm), and mechanical/surface texture) corresponding to three prominent sensory modalities. We found

strong evidence of MSI during larval settlement where the highest rates of settlement occurred in the presence of all three sensory cues and where the effects of cues changed in the presence or absence of other cues, resulting in a sensory cue hierarchy. Developmental transcriptome analyses revealed previously undescribed, deep homological links with bilaterian sensory system development and a peak expression of sensory transduction components for each of the three modalities in actinulae stage larvae. Lastly, RNA Fluorescent *in situ* Hybridization (FISH) studies localize several prominent sensory transcripts including opsin (photosensitivity), PKD2L1, and PKD1L3 (chemosensitivity), and ASIC, Piezo, and TRPA (mechanosensitivity) to cnidocytes and their attendant sensory neurons in competent actinulae. Our results demonstrate MSI in the brainless actinula of *E. crocea* and suggest that this capacity is facilitated by the activities of polymodal, chemo-photo-mechanoreceptive sensory neurons with distant ancestry to unimodal primary sensory neurons known from bilaterian animals.

Results

Larval nervous systems reach full development by the actinula stage of development

The actinula stage of *E. crocea* possesses morphological and cellular features such as the basal protrusion and tentacles replete with cnidocytes, that are associated with larval settlement (Yamashita 2003). However, the structure of the nervous system throughout larval development has not been examined. We examined larvae at four developmental stages, including the metamorphosed juvenile polyp stage, using immunohistochemistry (IHC) and confocal microscopy (Fig 1). The state of the nervous system at the earliest stage, the star embryo (Fig 1A), appears granular and undifferentiated, which we interpret as a contiguous assemblage of neural progenitor cells (Rentzsch et al. 2017). The larval nervous system becomes increasingly differentiated as development proceeds from the preactinula (Fig 1B) to the actinula stage (Fig 1C-F), whereupon the tentacles are loaded with neurons and cnidocytes (Fig 1F). Additionally, the basal protrusion, the structure that contacts the substrate during settlement, contains a concentrated ring of neural cells (Fig 1D). These data are consistent with the actinula stage being the competent stage for settlement and suggest that actinulae have the capacity to integrate sensory information using the tentacles and the basal protrusion.

Differences in the sensory environment impact larval settlement

Next, we investigated the sensory information actinula integrate in support of the settlement decision. We performed a factorial settlement study (Fig 2) assessing the impact of photosensory, chemosensory, and mechanosensory cues on larval settlement, which we analyzed using a three-way analysis of variance (ANOVA). Our experiment included 10 blocks (replicates) where each block had 28 treatments of all possible combinations of cues and examined a total of 2,800 individual actinula larvae (Fig 2A). While the blocking variable, which was the experimental day, did not influence the response, larval settlement did increase as the season progressed, similar to Yamashita et al (2003) (Fig S2). Each individual sensory cues significantly impacted settlement when assessed individually (light, p=0.0482; chemical, p=<2e-16; mechanical, p=<2e-16; Fig 2B-D; Table S1). Specifically, the rate of larval settlement increased significantly in the presence of

light compared to darkness (p=0.0482; Fig 2B), and in the presence of the chemical cue compared to its absence (p=<2e-16; Fig 2C) but decreased in the presence of a mechanical cue (p=<2e-16; Fig 2D), when no other cues were present.

The effect of photosensory cues on settlement (wavelengths of light) was investigated in the light-only treatment (Fig 2E) using contrast analyses, since this treatment included additional dimensions compared to chemical and mechanical cues (e.g., presence/absence of light, three wavelengths, and two intensities, totaling 7 light conditions; Fig 2A). Settlement increased in the presence of light compared to darkness (p=0.0027; Fig 2E and Fig 2B, Table S3). In addition, significantly higher settlement occurred in green wavelengths of light (p=0.00167; Fig 2E), whereas significantly lower settlement occurred in red wavelengths (p=0.01137; Fig 2E), compared to the other two wavelengths. No significant interaction between light intensity and light wavelength was detected.

Multisensory integration and a sensory cue hierarchy determine settlement in actinulae

Multisensory integration is detected by examining statistical interactions between different sensory conditions (Stein et al. 2009). Here we examined interactions between sensory cues as they relate to settlement rate using a three-way ANOVA and contrasts based on our experimental approach (Fig 2A; Table S4). No interaction between light and chemical cues was identified across experiments (p=0.33; 70 experiments total; Fig 2F and Fig 2I). Similarly, no significant interaction (p=0.89) was observed between light and mechanical cues (Fig 2G and Fig 2J). Conversely, chemical and mechanical cues displayed a significant positive interaction (p=<2e-16; Fig 2K). Alone, chemosensory cues were a strong determinant of larval settlement. However, in the combined presence of the mechanical cue, settlement rates were significantly enhanced, indicating an inversion in the sign of the mechanical cue in the presence of the chemical cue (biofilm). Recall that when the chemical cue was absent, the mechanical cue had a significant negative influence on settlement rate (p=<2e-16; Fig 2K).

The three-way interaction between photo-, chemo-, and mechanosensory cues from the ANOVA is also significant (p=0.022) and indicates MSI by enhancement (Stein et al. 2009). The multisensory response has a significantly higher mean than the largest unisensory response (chemosensory) and the chemo-mechanical response in the absence of light (Fig 3; Fig 2H; Fig 2L). Among the three-way interaction, larval settlement was significantly lower in darkness when chemical and mechanical cues were present (p=0.03; Fig 2H and L). Additionally, the rate of settlement is significantly higher in green light in the presence of chemical and mechanical cues (p=0.026), and significantly lower in red light (p=0.003; Fig 2H and L). This interaction can be seen in Fig 2L, which shows that green light at both intensities induce higher settlement rates under chemical, and mechanical cues, and lower settlement rates occur in red light. Together, the Area under curve (AUC) data for the different combinations of cues depict a sensory cue hierarchy (Fig 3) where the highest rates of settlement occur in the presence of light, chemical, and mechanical cues.

176 **Sensory gene expression peaks in competent larvae and diminishes during and after**
177 **metamorphosis**
178
179 We performed a comparative transcriptome study on six developmental stages of *E. crocea,* from
180 star embryo to metamorphosed juvenile polyp, to assess genetic correlates of the observed
181 sensory response. Illumina Hi-seq sequencing resulted in an average of 38 million reads per
182 replicate, with six replicates for each of the six developmental stages. We first used orthology
183 analyses to place assembled *E. crocea* transcripts into orthogroups that included sequence data
184 from a selection of metazoan genomes including human. We then used the Gene Set Enrichment
185 Analysis (GSEA) database (Subramanian et al. 2005; Liberzon et al. 2011, 2015) and EdgeR to
186 identify transcripts with significant differences in expression between any developmental stage
187 that were present in three gene sets: Sensory perception of light stimulus (212 genes in gene set;
188 Fig 4A), Sensory perception of chemical stimulus (501 genes in gene set; Fig 4B), and sensory
189 perception of mechanical stimulus (164 genes in gene set; Fig 4C).
190
191 Gene expression for both the photo- and mechanosensory gene sets share similarities across
192 larval development (Fig 4). First, genes involved in neurogenesis, cellular morphogenesis, and
193 sensory cell type specification show maximum expression early and peak at stage 2 of
194 development (preactinula). Examples of these for the sensory perception of light stimulus gene
195 set include *E. crocea* homologs of SEMA5B (axonal guidance), homologs of CRX, VSX1, VSX2, and
196 RAX2 (transcription factors, photoreceptor specification), NRL2E3 (transcription factor, rod
197 specification), RRH (opsin, detection of light) and others (Fig 4A). A similar pattern is observed
198 for the perception of mechanical stimuli gene set and include *E. crocea* homologs of MYH14 (cell
199 shape and cytokinesis), EPS8L2 (stereocilia maintenance), DRGX (nociceptive sensory neuron
200 development) and others (Fig 4C).
201
202 Next, a later pulse of gene expression associated with sensory physiology, cellular structure and
203 morphogenesis, and another round of sensory cell type specification characterizes both gene
204 sets. Examples of these later expressed transcripts for the perception of light stimuli gene set
205 include homologs of GUCY2F and RRH (phototransduction), MYO3B (photoreceptor cell
206 maintenance), ADGRV1 (development of hearing and vision), CNNM4 (retinal function), WHRN
207 (periciliary membrane complex maintenance), and POU4F2 (retinal ganglion cell development).
208 Genes that peak at stages 3 and 4 (actinula) from the perception of mechanical stimuli gene set
209 include CLIC5 (stereocilia formation), MYO3B (cochlear hair bundle morphogenesis), POU4F2
210 (terminal differentiation of hair cells), SLC25A5 (motor protein, modulates auditory stimuli),
211 ASIC2-3 (mechanoreception, potentiated by FMRFamide-related peptides), TRPA1
212 (mechanoreceptor transduction channel), and PIEZO2 (component of a mechanosensitive
213 channel). Finally, transcript expression for both gene sets strongly diminishes at stages 5 and 6,
214 which correspond to metamorphosis and the establishment of the primary polyp. This drop-off
215 in expression is specific to the sensory gene sets used to interrogate our data and is not a general
216 feature of our transcriptome data (Fig S3, Table S5). It is noteworthy that many of the transcripts
217 that show differential expression in development for either the photo- or mechanosensory gene
218 sets have shared functions in both.
219

Similar analyses for the sensory perception of chemical stimulus gene set indicate a markedly different trend as few developmentally differentially expressed transcripts were recovered for this set (Fig 4B). However, they do indicate strong stage 4 (actinula) differential expression of homologs of both PKD2L1 and PKD1L3, which dimerize and facilitate sour taste perception in mammals (Ishimaru et al. 2006; Fain 2020).

RNA Fluorescent *in situ* hybridization reveal evidence for polymodal sensory cells

Our studies of larval nervous system development, settlement behavior, and developmental transcriptomics portray an inflection of sensory capacity at stage 4 when actinulae are competent to settle. In order to elucidate the cell types associated with enhanced sensory capacity, and potential cellular partitioning among the different sensory modalities, we conducted fluorescent *in situ* hybridization (FISH) using RNA probes against selected, highly differentiated sensory transcripts (Fig 4) in stage 4 *E. crocea* actinulae. Our targeted transcripts include opsin (Ec_t.72976, photoreception), Piezo and TRPA1 (Ec_t.17544 and Ec_t.66269 respectively, mechanotransduction), and ASIC, PKD2L1, and PKD2L3 (Ec_t.82119, Ec_t.81080 and Ec_t.66208 respectively, chemotransduction). We examined the cellular and spatial expression of these transcripts using the opsin probe as a reference present in all FISH experiments. Confocal optical sections (0.2 μm) indicate strong colocalization between opsin (Fig 5 A-I), PKD1L3 (Fig 5 A and C) PKD2L1 (Fig 5 D, F, G, I), and ASIC (Fig 5 A and B) in sensory neurons that are adjacent to cnidocytes in all experiments. Conversely, Piezo is strongly expressed in cnidocytes, with weaker expression of opsin also detected in cnidocytes (Fig 5 G-I). Finally, opsin and PKD2L1 show some co-expression with TRPA, but most TRPA expression is observed in cnidocytes to the exclusion of opsin and PKD2L1, which are expressed primarily in sensory neurons (Fig 5 D-F). Our results were confirmed by quantifying colocalization using Manders' Overlap (Fig S4).

Discussion

Competence to settle is associated with cnidocyte and nervous system maturation

Our immunohistochemical analysis demonstrates that actinula (stage 4) larvae possess an elaborated nervous system with an abundance of cnidocytes located at the tips of the aboral tentacles and the basal protrusion. This is consistent with the findings of Yamashita et al. (2003), who described the cnidocyte composition of actinula larvae and showed that atrichous isorhizas are used to temporarily attach to surfaces in a behavior referred to as nematocyte-printing. In hydrozoans like *E. crocea*, cnidocyte discharge is modulated by adjacent sensory neurons, with which they form synapses (Hobmayer et al. 1990; Anderson et al. 2004; Westfall 2004; Anderson and Bouchard 2009; Plachetzki et al. 2012). The cnidocytes that facilitate nematocyte printing are located in the tentacles and a ring of neurons is present at the basal protrusion located on the aboral end of actinulae (Fig 1D). The aboral region is also the site for sensory integration in other hydrozoan larvae (Matsushima et al. 2010; Tran and Hadfield 2013). We propose that the sensory interplay between cnidocytes and their adjacent sensory neurons facilitate sensory integration during settlement.

264 **A sensory cue hierarchy and MSI during the larval settlement decision**
265
266 Our larval settlement studies identified a sensory cue hierarchy, where the highest rates of
267 settlement occurred in the presence of chemical, mechanical, and light cues, with green light
268 being the most permissive to settlement (Fig 3). This is not surprising as marine invertebrate
269 larvae in general are known to integrate information from different modalities (Pawlik 1992;
270 Kawaii et al. 1997; Hadfield and Paul 2001; Holst and Jarms 2007; Hadfield 2011; Mason and
271 Cohen 2012; Strader et al. 2015; Whalan et al. 2015; Say and Degnan 2020). This type of sensory
272 integration, and the likelihood that some cues are more important than others, was the basis for
273 the proposal that a hierarchy of sensory cues dictates larval settlement in a species-specific
274 manner (Kingsford et al. 2002; Hodin et al. 2018). However, the existence of such a hierarchy has
275 not been experimentally validated until now. At the top of the sensory cue hierarchy for *E. crocea*
276 larval settlement are chemical cues produced by microbial biofilms. This is consistent with larval
277 settlement studies in other metazoan species (e.g., annelids: (Hadfield and Paul 2001; Harder et
278 al. 2002; Lau et al. 2002; Huang and Hadfield 2003; Huang et al. 2007; Hadfield 2011; Freckelton
279 et al. 2017); barnacles and bryozoans: (Qian et al. 2003; Faimali et al. 2004; Dobretsov and Qian
280 2006; Zardus et al. 2008; Dobretsov and Rittschof 2020)) that identified biofilm-derived cues for
281 larval settlement. It is likely that biofilm-derived chemical cues serve as a general indicator of
282 habitat quality across sessile metazoan species with dispersive larval stages (Wieczorek and Todd
283 1998; Lau et al. 2005; Hadfield 2011).
284
285 We also found a significant effect of light wavelength on larval settlement in *E. crocea*. Previous
286 work in hydrozoan species noted similar findings where animals are more sensitive to light in the
287 blue to blue–green spectrum compared to red light (Taddei-Ferretti et al. 2004; Guertin and Kass-
288 Simon 2015; Strader et al. 2015). In the case of *E. crocea* larval settlement, green light, which
289 penetrates only to shallow depths in the water column, may serve as a depth meter ensuring that
290 colonies of *E. crocea* settle at shallow depths where prey items like plankton are abundant. We
291 note that our finding of the preference of *E. crocea* larvae to settle in areas illuminated in green
292 light does not in itself indicate the capacity for discrimination between wavelengths of light in *E.*
293 *crocea* larvae. It is more likely that actinulae larvae are effectively "color blind" but show a higher
294 sensitivity to green light due to a limited photoreceptor palate with sensitivity in that range.
295 Indeed, we uncovered only two closely related opsin transcripts from *E. crocea* larval stages.
296
297 Many of the same sensory cues that we investigated here have been investigated previously in
298 other species. However, in most cases, studies have focused on one or two cues of interest (Svane
299 and Dolmer 1995; Nellis and Bourget 1996; Wieczorek and Todd 1998; Zardus et al. 2008; Mason
300 and Cohen 2012; Strader et al. 2015; Hodin et al. 2018; Say and Degnan 2020). Our factorial
301 experimental design allowed us to identify interactions between sensory modalities and to test
302 the possibility of MSI. Surprisingly, we found a significant interaction between mechanical
303 (surface texture) and chemical (biofilm) cues whereas, in the presence of chemical cues, surface
304 texture enhances settlement rates, but in the absence of chemical cues, surface texture is
305 inhibitory. This significant and sign-reversing sensory interaction constitutes MSI by
306 enhancement (Stein et al. 2009) and is likely mediated by signaling between sensory neurons and
307 their adjacent cnidocytes. MSI by enhancement is stronger when light is present in addition to

308 chemical and mechanical cues, suggesting that both photosensitivity and chemosensitivity have
309 positive impacts on settlement when mechanical cues are present.
310
311 **The cellular basis for MSI in actinulae**
312
313 Temporal patterns of gene expression also illuminate the sensory determinants of the settlement
314 decision in *E. crocea*. Our analytical approach, a type of GSEA, filtered transcripts based on their
315 phylogenetic membership into clades containing genes annotated as having sensory function and
316 then interrogated such transcripts based on their differential expression between stages. While
317 each of the three gene sets used for interrogation contained greater than 200 genes, only a
318 subset of those genes have orthologs in the *E. crocea* transcriptome and are differentially
319 expressed between stages (Fig 4). The mechanosensory gene set includes the largest number of
320 active genes while the chemosensory gene set contains the least number of genes. This disparity
321 is partly due to the relative degree of conservation in gene function between cnidarian genomes
322 and those of model organisms from which annotations are based, and partly due to genes that
323 are differentially expressed in *E. crocea* larval development. In addition, the mechanosensory and
324 photosensory gene sets share a number of genes in common due to pleiotropic expression. It is
325 somewhat surprising that so few chemosensory genes were recovered by our screen given that
326 chemosensitivity is the predominant sensory cue in larval settlement. However, we did identify
327 orthologs of both PKD1L3 and PKD2L1, which have been implicated as key components of the
328 sour taste (pH) transduction pathway in mammals (Ishimaru et al. 2006; Fain 2020) and have
329 previously been implicated in cnidarian chemosensitivity (McLaughlin 2017). Furthermore,
330 biofilms vary in acidity (Dexter and Chandrasekaran 2000), which could allow for the assessment
331 of different settlement sites based on their chemosensory properties.
332
333 These analyses identify two pulses of sensory gene expression: one occurring early (stage 2,
334 preactinula) and consisting largely of regulatory and structural factors and another occurring
335 later (stage 4, actinula) and consisting of structural and physiological factors. These data add
336 further support for the actinula (stage 4) as the maximally sensory-equipped larval stage and
337 highlight candidate genes for expression analyses.
338
339 We examined the expression of several candidate genes in stage 4 actinula larvae using FISH (Fig
340 5). We used the same opsin transcript (Ec_t.72976) in each experiment to facilitate comparisons
341 between genes. Our results demonstrate strong co-expression of opsin, PKD2L1, PKD1L3 and
342 ASIC in sensory neurons. In contrast, TRPA and Piezo transcripts localized to cnidocytes. These
343 results demonstrate cellular partitioning between the modes of sensation, where opsin
344 (photosensitivity) and PKD2L1, PKD1L3, and ASIC (chemosensitivity) are expressed in polymodal
345 sensory neurons, and TRPA and Piezo (mechanosensitivity) are expressed in cnidocytes.
346
347 Together, these data suggest that MSI in *E. crocea* larval settlement is facilitated by a simple
348 communication circuit between polymodal photo-chemo sensory neurons and
349 mechanoreceptive cnidocytes located on the tentacles and aboral basal protrusion. We propose
350 that in the absence of chemical and photosensory cues, mechanosensitive cnidocytes are
351 inhibited from discharging and little cnidocyte printing behavior takes place. However, when light

352 and chemical cues are present, this inhibition is relieved and mechanosensitive cnidocytes are
353 free to fire. The combination of permissive light, chemical, and mechanical cues lead to the
354 highest rate of settlement.
355
356 MSI is best known in animals with complex brains where specialized brain centers have evolved
357 to facilitate information processing and exchange. Here we show that MSI is possible in animals
358 that lack centralized nervous systems and may be facilitated by communication between as few
359 as two cell types, sensory neurons and cnidocytes. Moreover, given the importance of larval
360 settlement dynamics in shaping benthic ecosystems, it is likely that MSI as observed in *E. crocea*
361 larvae, may be an important determinant of benthic community composition and function.
362
363 **Conclusion**
364
365 Understanding how cnidarians integrate sensory information from the environment is critical to
366 understanding the ecological processes that dictate benthic community composition. At the
367 same time, uncovering the genetic determinants of cnidarian sensory behavior can illuminate the
368 deep evolutionary histories of the animal senses and provide clues on their early functions. We
369 show that brainless actinula larvae use multisensory integration (MSI) during the larval
370 settlement decision that incorporates information processing from the light, chemical and
371 mechanical senses. MSI is usually portrayed as a process involving information flow between
372 higher-level brain centers (Stein 1998; Otto et al. 2013; Stein et al. 2014; Ghosh et al. 2017;
373 Currier and Nagel 2020), however, our results indicate that MSI may be facilitated by interactions
374 between cells, and may have been a prominent feature of the organismal biology of metazoans
375 prior to the evolution of complex brains.
376
377 **Acknowledgments**
378 Research reported in this publication was supported through the University of New
379 Hampshire's Center for Integrated Biomedical and Bioengineering Research (CIBBR) through a
380 grant from the USDA.
381
382 **Author Contributions**
383 Conceptualization, D.P.; Methodology, D.P. and S.B.; Investigation, S.B.; Writing – Original Draft,
384 S.B.; Review & Editing, D.P. and S.B.; Funding Acquisition, D.P.; Resources, D.P.; Supervision,
385 D.P.
386
387 **Declaration of interests**
388 The authors declare no competing interests.
389
390 **Figures**

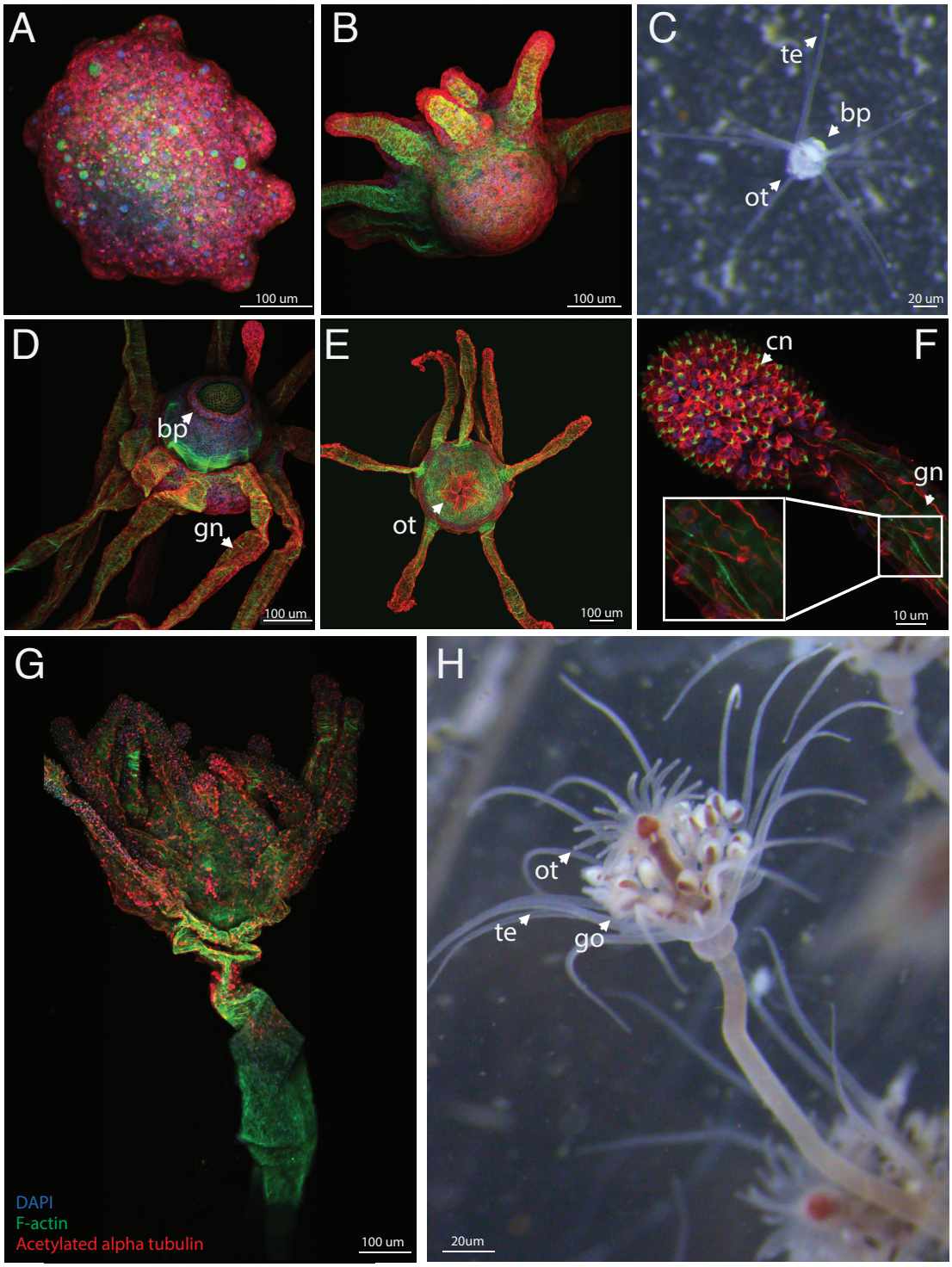

Figure 1. Nervous system development of *Ectopleura crocea* actinulae larvae
A,B,D-G Immunohistochemistry (IHC) staining of four developmental stages of *E. crocea* larvae where red staining corresponds to acetylated alpha-tubulin expression in neurons, green staining corresponds to contractile F-actin in muscles and stereocilia, and blue staining corresponds to DNA in nuclei. (**A**) Stage 1, star embryo. (**B**) Stage 2, preactinula. (**C**) Light micrograph of an

397 actinula larva. The arrows point to the basal protrusion (bp) which attaches to the substrate
398 during settlement, the tentacles (te), and the developing oral tentacles (ot). (**D**) The aboral end
399 of a Stage 3-4 actinula larva. The arrows point to the basal protrusion (bp) and ganglion neurons
400 (gn) in the tentacles. (**E**) Oral end of an actinula larva at stage 3-4. The arrow is pointing to the
401 developing oral tentacles (ot). (**F**) High magnification of a stage 3-4 actinula tentacle. An
402 abundance of cnidocytes (cn) are found at the tips of the tentacles. Additionally, ganglion
403 neurons (gn) extend down the tentacles and connect to the actinular nerve net. (**G**) A
404 metamorphosed juvenile polyp. (**H**) A light micrograph of an adult *E. crocea* polyp. The arrows
405 point to the oral tentacles (ot), the aboral tentacles (te), and the gonophores (go).
406

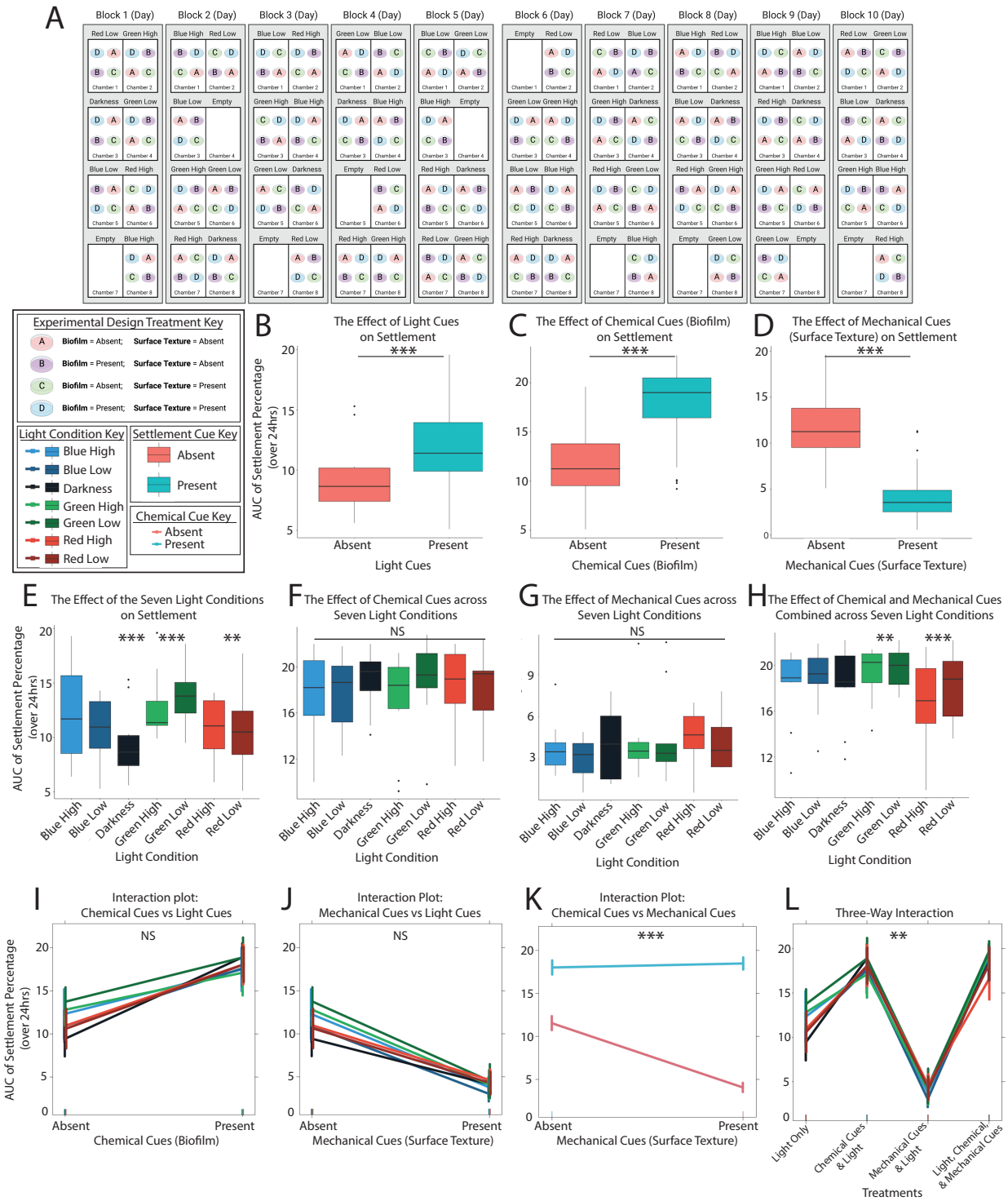

Figure 2. Settlement responses of actinula larvae to three sensory cues (**A**) Cartoon depiction of the larval settlement experimental design: 7x2x2 Split-plot Randomized Complete Block Design (RCBD) with 10 replicates. The block represents an experimental day which is also a replicate. We included all four combinations of presence and absence of biofilm and surface texture which are depicted as A-D treatments, where each biofilm and texture combination was exposed to all 7 light conditions in a single replicate. (**B**) The individual effect of

light cues on settlement. Larval settlement is significantly higher (p=0.0027) in the presence of a light cue compared to the absence of a light cue (darkness). (**C**) The individual effect of chemical cues (biofilm) on settlement. Larval settlement is significantly higher (p=<2e-16) in the presence of a chemical cue compared to the absence of one. (**D**) The individual effect of mechanical cues (surface texture) on settlement. Larval settlement is significantly lower (p=<2e-16) in the presence of a mechanical cue compared to the absence of one. (**E**) The effect of the seven light conditions on settlement. Larval settlement was significantly lower in darkness (p=0.00272) and in red wavelengths of light (p=0.01137) and significantly higher in green wavelengths of light(p=0.00167). (**F**) The effect of chemical cues (biofilm) across the seven light conditions. There were no significant differences in settlement in any wavelength of light (blue p=0.51; green p=0.60; red p=0.88) in the presence of a chemical cue. (**G**) The effect of mechanical cues (surface texture) across the seven light conditions. There were no significant differences in settlement in any wavelength of light in the presence of a mechanical cue (blue p=0.99; green p=0.79; red p=0.79). (**H**) The effect of chemical and mechanical cues combined across the seven light conditions. There was a significant increase in settlement in the presence of green wavelengths of light (p=0.02) and significantly lower settlement in red wavelengths of light (p=0.003). (**I**) The interaction of chemical cues and light cues. There was no significant interaction between these two cues (p=0.33). (**J**) The interaction between mechanical cues and light cues. There was no significant interaction between these two cues (p= 0.89). (**K**) The interaction between chemical and mechanical cues. There was a significant interaction between these two cues (p=<2e-16) with an additive effect in the presence of both cues. (**L**) The three-way interaction of chemical, mechanical, and light cues. Treatment A is the light cues only treatment, treatment B is light and chemical cues, treatment C is light and mechanical cues, and treatment D is all three cues. There is a significant three-way interaction (p=0.02).

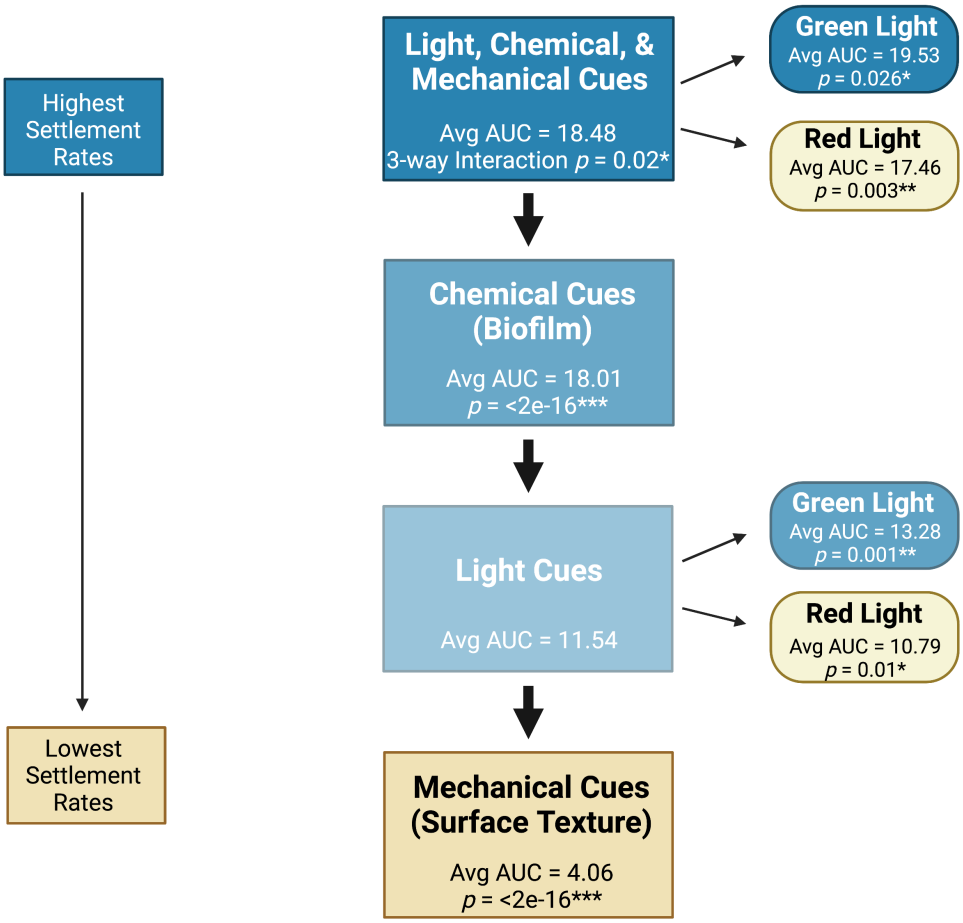

Figure 3. Sensory cue hierarchy of larval settlement in actinula larvae
The highest rates in settlement occur in the presence of all three cues, where significantly higher settlement rates occurred in the presence of green light, and significantly lower settlement rates occurred in the presence of red light. Following the combination of all three cues is the second tier composed of chemical cues which significantly increases larval settlement rates, but not to the same magnitude as having all three cues present. Light did not interact with chemical cues, leading to the lack of a light hierarchy in this second tier. The third tier is the light cues only treatment, where the highest rates of settlement occur in green light and the lowest rates occur in red light. Lastly, is the Mechanical cue tier which significantly decreased settlement rates. Additionally, the scale of color indicates the strength of a cue (darker colors indicate stronger influence).

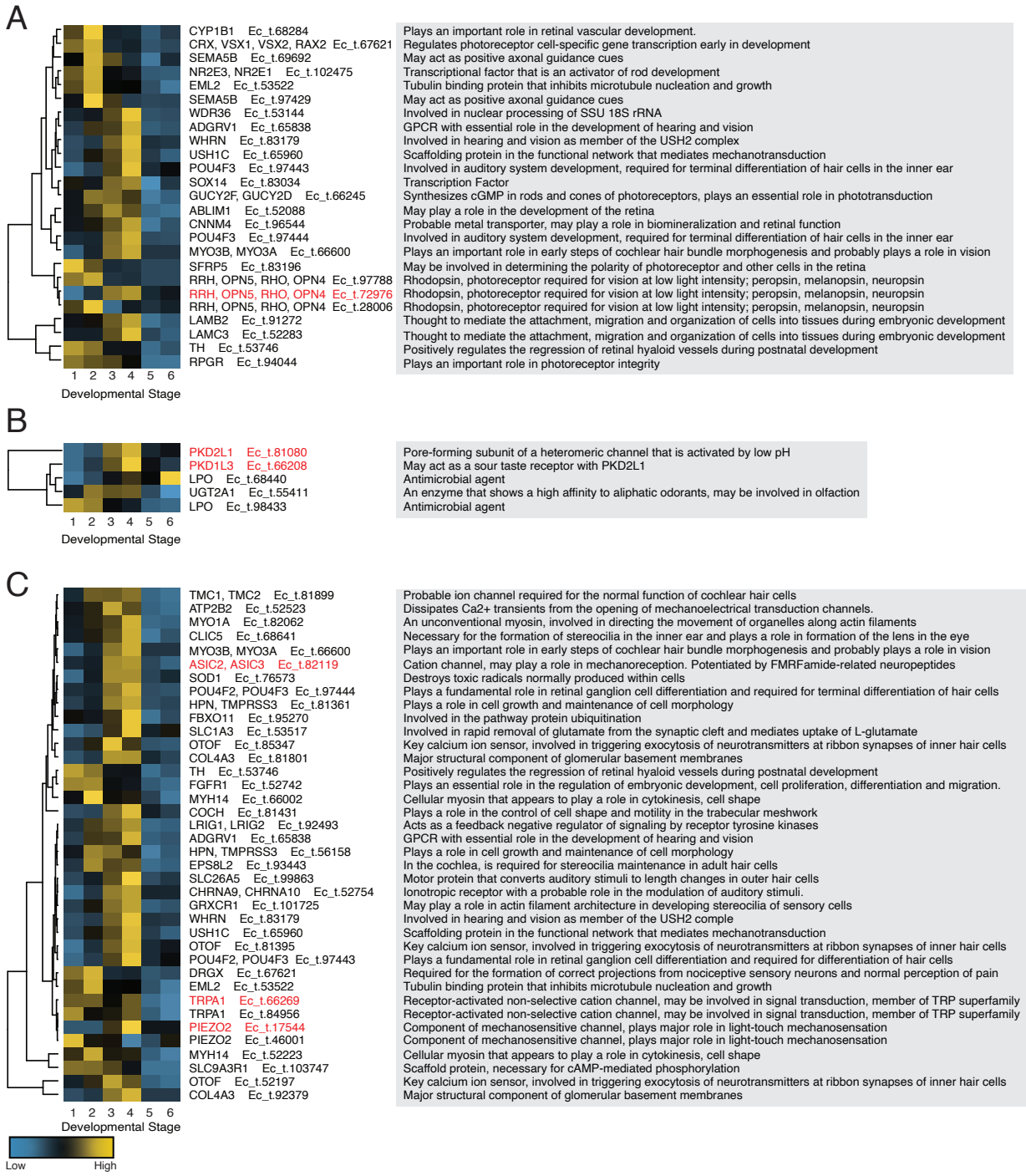

Figure 4. Gene expression over development in actinulae larvae for three sensory gene sets Heatmaps of significantly differentially expressed genes over development for the following three gene sets: (**A**) sensory perception of light stimulus; (**B**) sensory perception of chemical stimulus; and (**C**) sensory perception of mechanical stimulus. High expression is signified by yellow and low expression is light blue. The grey panels to the right contain abbreviated descriptions of gene functions from UniProt. The transcripts highlighted in red are the transcripts used to make RNA Fluorescent *in situ* hybridization probes. Gene trees of the orthogroups of probes can be seen in Figure S6. Developmental stages: 1 *star embryo*, 2 *preactinula*, 3 *young*

actinula, 4 *actinula in nematocyte-printing stage*, 5 *settled (attached) actinula*, 6 *metamorphosed juvenile polyp*.

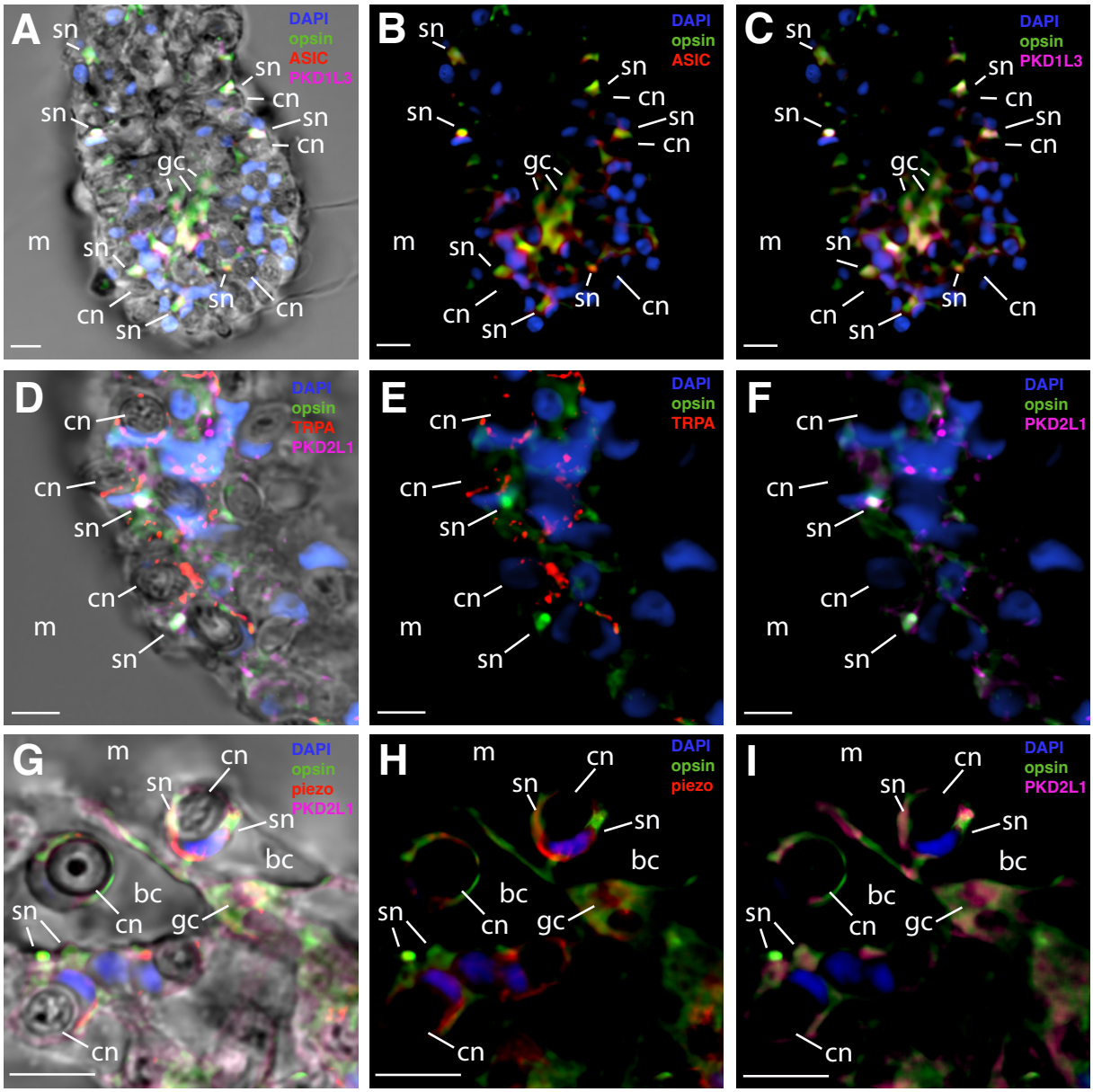

Figure 5. RNA fluorescent *in-situ* hybridizations (FISH) of sensory transcripts in actinulae tentacles (**A-C**) Same tissue where green is opsin, red is ASIC, cyan is PKD1L3, and blue is DAPI. (**A**) Merge of all confocal channels with the transmitted light (TD) channel. (**B-C**) The merge of confocal channels separated from transmitted light (TD). (**D-F**) Same tissue where green is opsin, red is TRPA, cyan is PKD2L1, and blue is DAPI. (**D**) Merge of confocal channels with the transmitted light (TD) channel. (**E-F**) The merge of confocal channels separated from the transmitted light (TD). (**G-I**) Same tissue where green is opsin, red is Piezo, cyan is PKD2L1, and blue is DAPI. (**G**) Merge of confocal channels with the transmitted light (TD) channel. (**H-I**) The merge of all confocal channels separated from the transmitted light (TD) at different sections of the sample.

474 Cnidocytes (cn), sensory neurons (sn), ganglion cell (gc), battery cell (bc), medium (sea water)
475 (m). All scale bars are 10um.
476
477 **Methods**
478
479 **Field collection of *E. crocea* Colonies**
480 Larva were obtained by collecting adult *E. crocea* colonies at the UNH Coastal Marine Lab (CML)
481 pier in New Castle, NH in June and July 2020. Colonies were transported to UNH in unfiltered sea
482 water immediately after collection. The colonies were cultured and maintained according to
483 Mackie (1966) where colonies were placed in large glass bowls for predator and dirt removal.
484 Once cleaned, colonies were moved to new bowls filled with unfiltered sea water and were
485 placed in an incubator with an aeration stone connected to a bubbler at a 12/12 L:D cycle at 18°C.
486 Colonies were undisturbed overnight to allow spawning and actinula release. Actinula were
487 identified and collected the following day for settlement experiments or for staining.
488
489 **Immunohistochemistry and Confocal Microcopy**
490 Immunohistochemistry was performed on four developmental stages: embryos, pre-actinulae,
491 actinula larvae, and juvenile polyps, which were obtained as described above. Samples were fixed
492 overnight at 4°C in 4% paraformaldehyde (Sigma) in PBST. We followed the protocol from
493 Plachetzki et al. (2012) with minor alterations for staining. Samples were washed five times with
494 5 minute incubations in PBST (3.2 mM Na2HPO4, 0.5 mM KH2PO4, 1.3 mM KCl, 135 mM NaCl,
495 0.1% Tween 20, pH 7.4) and blocked for 2 h in PBST + 20% normal goat serum (NGS; Sigma) at
496 room temperature. Samples were then incubated with primary antibody, anti-acetylated
497 α tubulin (1:500; Sigma), in blocking solution over night at 4°C. Following the primary antibody,
498 samples were washed five times with 5 min incubations in PBST and blocked as before. Samples
499 were then incubated with the secondary antibody, Cy2-conjugated anti mouse IgG (1:1000;
500 Jackson), and blocking reagent overnight at 4°C. Samples were then washed five times with 5 min
501 incubations in PBST. Afterwards, a solution containing Alexa Fluor 488-labeled phalloidin stock
502 (1:40; Invitrogen) in PBST was added for 1 h. Samples were then washed five times with 10 min
503 incubations and were then mounted in ProLong Antifade Mountant with DAPI (ThermoFisher).
504 Samples were imaged on the UNH Nikon A1R HD confocal Microscope.
505
506 **Larval Settlement Study Experimental Design and Materials**
507 The larval settlement study was designed as a 7x2x2 split-plot Randomized Complete Block
508 Design (RCBD) with 10 blocks, Fig 1A. The blocking variable was the experimental day that
509 replicates were performed on where larvae in one block were from colonies collected at the same
510 time and location the day prior to the experiment. The purpose of the blocking variable was to
511 account for environmental variation between colonies and days across the study, and each block
512 contained all 28 treatments. An experimental unit was a single petri dish that contained 10
513 actinula larvae, this allowed us to use the area under the curve (AUC) as our response variable.
514 The three treatment factors were the sensory cues of interest which included seven levels of light
515 conditions, two levels of chemosensitive treatments, and two levels of mechanosensitive
516 treatments. Replicates were performed in four hand-made light boxes where each light box had
517 two chambers (described below). The first randomization of the split-plot design, which was

applied at the chamber level, were the seven light conditions described in Table 1. The second randomization was comprised of the chemical and mechanical cues and were applied at the petri-dish level in a factorial presence/absence structure and can be seen in Table 2.

Table 1. The seven levels of the light condition factor with their corresponding measurements

Light Conditions in Study	Wavelength	Intensity
Red Light, High Intensity	630nm	10 µmol m-2 s-1
Red Light, Low Intensity	630nm	5 µmol m-2 s-1
Green Light, High Intensity	520 nm	10 µmol m-2 s-1
Green Light, Low Intensity	520 nm	5 µmol m-2 s-1
Blue Light, High Intensity	460nm	10 µmol m-2 s-1
Blue Light, Low Intensity	460nm	5 µmol m-2 s-1
Darkness	0nm	0 µmol m-2 s-1

Table 2. Factorial Structure of Chemical and Mechanical Cue Dish Treatments

	Chemical Cue Absent	**Chemical Cue Present**
Mechanical Cue Absent	Dish Treatment A	Dish Treatment B
Mechanical Cue Present	Dish Treatment C	Dish Treatment D

Prior to settlement experiments, four five-sided light boxes were created with black opaque acrylic (Acrylite; Extruded 9M001) with a thickness of 0.177 inch (in) and 16in x 12in x 12in dimensions with two centered, circular holes with diameters of 85mm cut out of the top. An additional piece of acrylic with the same thickness with 12in x 12in dimensions was placed in the center of the box to create two separate chambers. Super Bright LEDs heatless lights (part #: WRLFA-RGB6W-60) were placed in the cutout holes which allowed control of four different light intensity settings for the wavelengths red (630 nm), green (520 nm), and blue (460 nm). Light intensity was measured using an LI-1000 DataLogger. For replicability the boxes were placed in the same position for each replicate. The positions of petri-dishes were also marked at high and low intensities for each wavelength in each chamber for replicability, Fig S1B.

To obtain chemical cues, we allowed petri-dishes to generate biofilms by placing dishes in mesh dive bags and attached them to the UNH CML pier for 1 week at a depth of 1.5 m (Lee et al. 2008, 2014). Colonized dishes were then transported to the laboratory in seawater collected at the site and were used in settlement studies and for biofilm sequencing (Corcoll et al. 2017). To obtain mechanical stimuli, petri-dishes were scratched by 36-Grit Ceramic Alumina Sandpaper (Lowes; Model #: 9150-052) in a circular motion on the outer part of the dish, then with three scratches, non-overlapping, going from one side to the other in the center of the dish to ensure full coverage. Dishes were then rinsed twice, once with DI water to remove any plastic shavings, and then a second time with sea water immediately prior of use in a replicate to ensure removal of plastic shavings.

Larval Settlement Study

Larva were obtained by collecting adult *E. crocea* colonies at the UNH CML pier in New Castle, NH in June and July 2020. Colonies were cultured and maintained according to Mackie (1966) as

551 described above. Colonies of *E. crocea* were undisturbed overnight (12-15 hours) to allow
552 spawning and actinula release. The following day, larvae at the actinula stage were collected and
553 placed in 100mm x 15mm plastic petri dishes (Thermo Scientific) where each petri dish contained
554 10 larvae and the dish treatments corresponded to the predetermined randomized dish
555 conditions for the 28 experimental treatments. Larvae were identified under a microscope
556 following Yamashita et al. (2003) where we sought out young actinula with stiff tentacles, small
557 and circular bodies, and short aboral poles.
558
559 One block (replicate) of all 28 treatment conditions began once larvae were collected at the
560 actinula stage where start times were staggered by chamber which had four petri dishes with a
561 total of 40 larvae. Dishes from the four chemical and mechanical treatment conditions were
562 placed at the appropriate positions and wavelength and light intensity were adjusted according
563 to the predetermined randomized treatment conditions per chamber. Metamorphic stages were
564 recorded at the following time points: 0 hours (hrs), 2hrs, 4hrs, 6hrs, 8hrs, 12hrs, and 24hrs. At
565 each time point, dishes were taken out of the light box and placed under a microscope where
566 each individual larva was observed and quantified based on their metamorphic stage (detailed
567 below). Immediately following quantification, the replicate dish was placed back into the light
568 box until the next time point for quantification, this procedure was performed for each of the 28
569 dishes at each time point.
570
571 Larval quantification was assessed on a presence/absence metamorphosis scale with three
572 levels. A 0 signified larvae were still in the actinula phase and had not metamorphosed or settled,
573 a 1 indicated that larvae had settled (attached to the substrate but had not completed
574 metamorphosis), and a 2 signified that larvae had completed metamorphosis into a juvenile
575 polyp. At each time point, we counted and recorded the total number of larvae for each condition
576 under the scale. From this information, we then calculated the area under the curve using the
577 settlement percentages at each time point, which combined the number of settled and
578 metamorphosed larvae (# of Settled + # of Metamorphosed/total # of larvae in dish). The
579 following equation was used to calculate the area under the curve (AUC) which was used as the
580 response variable in statistical analyses (Mohapatra et al, 2014; Shaner, 1977):
581
582 $$\text{AUC} = \sum_{i=1}^{n}[(y_i + y_{i+1})/2] * [t_{i+1} - t_i]$$
583
584 Where y_i is the proportion of settled and metamorphosed larvae at the ith time point; t_i is the
585 timepoint in hours where larvae were observed, and n is the total number of observations per
586 petri-dish in a replicate. Normally distributed data were compared statistically by a split-plot
587 RCBD three-way analysis of variance (ANOVA) and with orthogonal contrasts in the R
588 environment.
589
590 **Library preparation, sequencing and read processing**
591 Colonies of *E. crocea* were collected at the UNH CML pier in May and June 2019. Colonies were
592 maintained and larva were obtained as previously mentioned above. We collected six replicates
593 of the six developmental stages: embryos, pre-actinula, actinula (younger), settling actinula
594 (older), settled actinula, and metamorphosed juvenile polyps (Yamashita 2003), where each

595 stage had a total of 125 larva collected. Samples were stored in RNA*later* (Thermo Fisher
596 Scientific) in -20°C until total RNA was extracted using the PureLink RNA Mini Kit (Thermo Fisher
597 Scientific; Cat no. 12183018A) according to the manufacturer's instructions and quantified using
598 NanoDrop (Thermo Scientific). Libraries were created using 1000ng of total RNA with the
599 NEBNext Ultra 2 Directional RNA Library Kit following the Poly(A) mRNA Magnetic Isolation
600 module (NEB #E7490). Libraries were sent to Novogene for Illumina Hi-Seq. After sequencing,
601 reads were processed using custom python scripts which executed FastQC and selected the
602 highest quality replicate for each of the 6 stages. It then concatenated the highest quality
603 replicate for each of the 6 stages to generate representative R1 and R2 read files to be used in *de*
604 *novo* transcriptome assembly. The Oyster River Protocol (ORP) was used as the assembler which
605 performs read trimming, read normalization, read error correction, and generates an assembly
606 using a multi-kmer and multi-assembler approach and then merges those assemblies into one
607 final high-quality assembly (MacManes 2018). The ORP also produced quality metrics from
608 TransRate and BUSCO.
609
610 **Gene expression analysis**
611 To prepare for gene expression analyses performed later in the workflow, two sub-steps were
612 completed. First, the program Salmon was executed to quantify transcripts in the linux
613 environment (Patro et al., 2017). Next, EdgeR was implemented in the R environment to identify
614 significant differential gene expression between pair-wise comparisons of the six developmental
615 stages (Chen et al. 2020). Count data was reduced by requiring transcripts to have 10 counts in a
616 library to be considered expressed and were filtered by counts-per-million (CPM)(Chen et al.
617 2020). The calcNormFactors function was used to normalize library sizes which used a trimmed
618 mean of M-values (TMM) method. To estimate dispersion, a quantile-adjusted conditional
619 maximum likelihood (qCML) method was employed. Differentially expressed genes (DEGs) were
620 identified at a p-value of 0.05 and results from each comparison was exported to the terminal
621 and included the transcript header, logFC, logCPM, PValue, and FDR which was used in a later
622 step.
623
624 TransDecoder was then implemented to translate the assembly from nucleotide space into
625 protein space. To reduce the amount of duplicate protein models, we ran cd-hit on the actinula
626 protein FASTA. The reduced actinula FASTA was then used in OrthoFinder along with the
627 following taxa from publicly available data on NCBI: *Homo sapiens*, *Drosophila*, *Hydra*,
628 *Hydractinia* (adult and larval forms), and *Nematostella*.
629
630 While OrthoFinder was running, we obtained sensory gene sets from the Gene Set Enrichment
631 Analysis (GSEA) created by the Broad Institute and UC San Diego (Subramanian et al. 2005;
632 Liberzon et al. 2011, 2015). We selected the following three gene sets:
633 GO_Sensory_Percep_Of_Light_Stimulus, GO_Sensory_Perception_of_Chemical_Stimulus, and
634 GO_Sensory_Perception_of_Mechanical_Stimulus. We then imported the Entrez IDs, gene
635 symbols, and descriptions of the members in the gene sets as a CSV file into the terminal. Using
636 custom made python scripts we reformatted the gene set information and searched the Entrez
637 IDs using the Bio.Entrez module in python to obtain the protein sequences for each gene across
638 the three gene sets.

639
640 Our human protein sequences used in OrthoFinder contained altered headers, therefore we
641 performed three BLASTp searches on our human protein sequences using the genes from the
642 sensory gene sets as queries. The search allowed one target sequence result at an e-value of
643 0.00001. The output from the three searches included the official NCBI headers and the
644 corresponding altered header used in our human protein models. This was used to annotate the
645 altered human protein models used in OrthoFinder with the various sensory genes in the
646 following step. Additionally, we generated another output file that was composed of human
647 sequence IDs from the NCBI database and their corresponding gene symbols.
648
649 To identify actinula transcripts that shared orthogroups with human transcripts of sensory genes,
650 we imported the following results into the R environment to be used in a custom R script:
651 OrthoFinder (orthogroup.tsv file and counts file), the BLAST results with the two human headers
652 (NCBI and the altered headers used in our human protein FASTA), and the file with the NCBI
653 headers and its corresponding gene symbol. This R script then identified and re-labeled the
654 orthogroups that contained the genes from the sensory gene sets with the gene symbols and
655 reported the actinula transcripts that were contained in those orthogroups with the gene symbol
656 labels. The lists of actinula headers with their corresponding gene symbols were exported from
657 R into the terminal and were used with a custom python script and the edgeR output to identify
658 significantly differentially expressed genes within the gene sets. The significant DEGs were then
659 visualized as heatmaps for each gene set in the R environment.
660
661 **RNA Fluorescent *in situ* Hybridization Study**
662 Sequences were identified to make RNA probes for *in situ* hybridizations using the transcriptomic
663 expression data from the developmental transcriptome study. We identified the highest
664 expressed transcripts of key sensory genes from the three sensory gene sets. We then designed
665 RNA-probes for our target sequences using the Stellaris RNA FISH platform (Biosearch
666 Technologies) with the custom probe design service following their recommendations for probe
667 design.
668
669 Actinula larvae were obtained as previously described above. Samples were stained according to
670 the Stellaris FISH protocol with alterations to the protocol. Samples were fixed overnight at 4°C
671 in 4% paraformaldehyde (Sigma) in PBS. The following day samples were washed five times with
672 5 minute incubations in PBST. Samples were then incubated in Prot K (1ug/ul) for 10 minutes at
673 room temperature. Immediately following the Prot K incubation, the solution was removed, and
674 samples were incubated in glycine (4ug/ul) for 10 minutes at room temperature to stop the Prot
675 K reaction. Samples were then washed twice with 5 minute incubations in PBST. We then refixed
676 samples in 4% PF for 30 minutes at room temperature. Following refixation, samples were
677 washed five times with 5 minute incubations in PBST. We then transferred samples to 1.5ml
678 microcentrifuge tubes and incubated samples in Wash Buffer A (Catalog# SMF-WA1-60) for 5
679 minutes at room temperature. We then ran a prehybridization step using the stellaris
680 hybridization buffer (Catalog# SMF-HB1-10) at 37C for 1 hour in a shake 'N' bake Hybridization
681 Oven. Following the prehybridization step, we added the hybridization buffer with probes (10ul
682 of each probe for a total of 30ul of probe) to our samples and incubated them at 37C overnight

683 in the dark. The following day, the hybridization buffer with probe solution was removed and
684 samples were incubated in Wash Buffer A at 37C for 30 minutes in the dark. Samples were then
685 incubated in Wash buffer B (Catalog# SMF-WB1-20) for 5 minutes at room temperature in the
686 dark. We resuspended samples in PBST and mounted them in ProLong Antifade Mountant with
687 DAPI (ThermoFisher). Samples were imaged on the UNH Nikon A1R HD confocal Microscope.
688
689 **Supplemental Information titles and legends**
690
691 **Figure S1.** Experimental setup for actinula settlement study
692 **(A)** The lightboxes used in the experiment. Each lightbox had two separate chambers where each
693 chamber had its own light source which could be changed to specific wavelengths of light and
694 intensity as demonstrated in (**B**).
695
696 **Figure S2.** Block interactions of actinula settlement study
697 (**A**) The interaction between chemical cues and the blocking variable (experimental day). There
698 is a significant interaction (p=0.002) occurring, however this figure depicts that the magnitude of
699 the response to chemical cues is maintained over time (the blocking variable). (**B**) The interaction
700 between mechanical cues and the blocking variable (experimental day). There is a significant
701 interaction (p=0.005) occurring, however the magnitude of the two responses is the same, the
702 lines do not intersect, which indicates that the blocks are not influencing the treatments.
703
704 **Figure S3.** Word Clouds of GO terms from significantly upregulated genes in actinula stages 5 and
705 6
706 (**A**) The GO terms for the significantly differentially expressed genes upregulated in stage 5,
707 settled larvae. Created using ReviGO. (**B**) The GO terms for the significantly differentially
708 expressed genes upregulated in stage 6, metamorphosed juvenile polyps. Created using ReviGO.
709 Also see Table S5 for a list of significant GO terms.
710
711 **Figure S4.** Quantification of Fluorescent *in-situ* Hybridization colocalization in actinula larvae
712 using Manders' Overlap
713 To quantify colocalization in the fluorescent *in-situ* Hybridization study, we performed a
714 Manders' overlap analysis which identifies the percentage that pixels overlap. (**A**) Depicts the
715 region of interest (ROI) where the Manders' overlap was performed for the staining of Opsin
716 (EGFP), Piezo (RFP), and PKD2L1 (CY5). The first row in the table details the percentage of overlap
717 for this experiment for each channel comparison. (**B**) Depicts the region of interest (ROI) for the
718 staining of opsin (EGFP), TRPA (RFP), and PKD2L1 (CY5). The second row in the table details the
719 percentage of overlap for this experiment. (**C**) Depicts the region of interest for the staining of
720 opsin (EGFP), ASIC (RFP), and PKD1L3(CY5). Across all experiments, DAPI stained cell nuclei blue.
721 All scale bars are 10um.
722
723 **Figure S5.** Control for RNA Fluorescent in-situ Hybridizations
724 To confirm that the staining from Figure 5 was actual signal, we performed a control experiment
725 where samples underwent the same protocol apart from adding RNA probes. A-J Two images of

726 different control samples. (A&F) Merged images of all the channels. (B&G) The RFP channel.
727 (C&H) The CY5 channel. (D&I) The GFP channel. (E&J) DAPI staining cell nuclei in blue.
728
729 **Figure S6**. Orthogroup gene trees of sequences used as RNA FISH Probes
730 The gene trees from Orthofinder for each of the 6 RNA FISH probes. Red indicates the transcript
731 used as a probe. Green indicates an actinula transcript that was significantly differentially
732 expressed (DE). Blue and the other colors represent the annotated human sequences from the
733 gene set.
734
735 **Table S1**. Three-way ANOVA from actinula larva settlement study (7x2x2 split-plot RCBD)
736 The main plot (first randomized variable) is the light condition and the sub plot (second
737 randomized variable) is the dish treatments which are set up in a factorial structure of
738 presence/absence of chemical (biofilm) and mechanical (surface texture) cues.
739
740 **Table S2**. Block interaction investigation from actinula larva settlement study (7x2x2 split-plot
741 RCBD)
742 We probed the block interaction because the blocking variable in Table S1 was significant. This
743 ANOVA examines if the blocking variable interacts with the treatment variables.
744
745 **Table S3**. Photosensory contrasts in light-only treatment from the actinula larva settlement study
746 Three separate contrasts were run, one for each wavelength of light, and are grouped together
747 in this single table. We asked four questions: Is there a difference in larval settlement when larvae
748 are (1) exposed to light compared to darkness; (2) in high-intensity light compared to low-
749 intensity light? (3) Is there a difference in larval settlement when larvae are in green light
750 compared to Blue & Red (Blue vs Green & Red, and Red vs Blue & Green); and (4) Is there a
751 difference in settlement when larvae are exposed to green light at a high intensity vs low intensity
752 (in blue light at high vs low; and red light at high vs low).
753
754 **Table S4**. Photosensory Contrasts for all interactions from the actinula larva settlement study
755 Three separate contrasts were run, one for each wavelength, and are grouped together. Here we
756 asked the same photosensory questions but are probing all two-way and the three-way
757 interactions.
758
759 **Table S5**. Actinula stages 5 and 6 significantly upregulated GO terms used in ReviGO analysis
760 (Supek et al. 2011).
761 We identified all genes that were significantly upregulated across these two stages and ran
762 Interproscan to identify GO terms. These are the resulting GO terms that we input to ReviGO to
763 generate word clouds of potential functions.
764
765 **References**
766 Alvarado JC, Vaughan JW, Stanford TR, Stein BE (2007) Multisensory versus unisensory
767 integration: Contrasting modes in the superior colliculus. J Neurophysiol 97:3193–3205.
768 https://doi.org/10.1152/jn.00018.2007
769 Anderson PAV, Bouchard C (2009) The regulation of cnidocyte discharge. Toxicon 54:1046–

770 1053. https://doi.org/10.1016/j.toxicon.2009.02.023
771 Anderson PA V, Thompson LF, Moneypenny CG, et al (2004) Evidence for a Common Pattern of
772 Peptidergic Innervation of Cnidocytes. Biol Bull 207:141–146
773 Chen Y, McCarthy D, Ritchie M, et al (2020) edgeR: differential analysis of sequence read count
774 data User's Guide. R Packag 1–121
775 Corcoll N, Österlund T, Sinclair L, et al (2017) Comparison of four DNA extraction methods for
776 comprehensive assessment of 16S rRNA bacterial diversity in marine biofilms using high-
777 throughput sequencing. FEMS Microbiol Lett 364:1–9.
778 https://doi.org/10.1093/femsle/fnx139
779 Currier TA, Nagel KI (2020) Multisensory control of navigation in the fruit fly. Curr Opin
780 Neurobiol 64:10–16. https://doi.org/10.1016/j.conb.2019.11.017
781 Dexter SC, Chandrasekaran P (2000) Direct measurement of ph within marine biofilms on
782 passive metals. Biofouling 15:313–325
783 Dobretsov S, Qian PY (2006) Facilitation and inhibition of larval attachment of the bryozoan
784 Bugula neritina in association with mono-species and multi-species biofilms. J Exp Mar Bio
785 Ecol 333:263–274. https://doi.org/10.1016/j.jembe.2006.01.019
786 Dobretsov S, Rittschof D (2020) Love at First Taste : Induction of Larval Settlement by Marine
787 Microbes
788 Faimali M, Garaventa F, Terlizzi A, et al (2004) The interplay of substrate nature and biofilm
789 formation in regulating Balanus amphitrite Darwin, 1854 larval settlement. J Exp Mar Bio
790 Ecol 306:37–50. https://doi.org/10.1016/j.jembe.2003.12.019
791 Fain GL (2020) Taste. In: Sensory Transduction, 2nd edn. Oxford University Press, pp 159–177
792 Freckelton ML, Nedved BT, Hadfield MG (2017) Induction of Invertebrate Larval Settlement;
793 Different Bacteria, Different Mechanisms? Sci Rep 7:1–11.
794 https://doi.org/10.1038/srep42557
795 Ghosh DD, Nitabach MN, Zhang Y, Harris G (2017) Multisensory integration in C. elegans. Curr
796 Opin Neurobiol 43:110–118. https://doi.org/10.1016/j.conb.2017.01.005
797 Guertin S, Kass-Simon G (2015) Extraocular spectral photosensitivity in the tentacles of Hydra
798 vulgaris. Comp Biochem Physiol -Part A Mol Integr Physiol 184:163–170.
799 https://doi.org/10.1016/j.cbpa.2015.02.016
800 Hadfield M, Paul V (2001) Natural Chemical Cues for Settlement and Metamorphosis of Marine-
801 Invertebrate Larvae
802 Hadfield MG (2011) Biofilms and Marine Invertebrate Larvae: What Bacteria Produce That
803 Larvae Use to Choose Settlement Sites. Ann Rev Mar Sci 3:453–470.
804 https://doi.org/10.1146/annurev-marine-120709-142753
805 Harder T, Lau SCK, Dahms HU, Qian PY (2002) Isolation of bacterial metabolites as natural
806 inducers for larval settlement in the marine polychaete Hydroides elegans (HASWELL). J
807 Chem Ecol 28:2029–2043. https://doi.org/10.1023/A:1020702028715
808 Hobmayer E, Holstein TW, David CN (1990) Tentacle morphogenesis in hydra. II. Formation of a
809 complex between a sensory nerve cell and a battery cell. Development 109:897–904.
810 https://doi.org/10.1242/dev.109.4.897
811 Hodin J, Ferner M, Heyland A, Gaylord B (2018) I feel that! Fluid dynamics and sensory aspects
812 of larval settlement across scales. In: Evolutionary Ecology of Marine Invertebrate Larvae.
813 pp 190–207

814 Holst S, Jarms G (2007) Substrate choice and settlement preferences of planula larvae of five
815 Scyphozoa (Cnidaria) from German Bight, North Sea. Mar Biol 151:863–871.
816 https://doi.org/10.1007/s00227-006-0530-y
817 Huang S, Hadfield MG (2003) Composition and density of bacterial biofilms determine larval
818 settlement of the polychaete Hydroides elegans. Mar Ecol Prog Ser 260:161–172.
819 https://doi.org/10.3354/meps260161
820 Huang YL, Dobretsov S, Xiong H, Qian PY (2007) Effect of biofilm formation by
821 Pseudoalteromonas spongiae on induction of larval settlement of the polychaete
822 Hydroides elegans. Appl Environ Microbiol 73:6284–6288.
823 https://doi.org/10.1128/AEM.00578-07
824 Ishimaru Y, Inada H, Kubota M, et al (2006) Transient receptor potential family members
825 PKD1L3 and PKD2L1 form a candidate sour taste receptor. Proc Natl Acad Sci U S A
826 103:12569–12574. https://doi.org/10.1073/pnas.0602702103
827 Kawaii S, Yamashita K, Nakai N, Fusetani N (1997) Intracellular calcium transients during
828 nematocyst discharge in actinulae of the hydroid, tubularia mesembryanthemum. J Exp
829 Zool 278:299–307. https://doi.org/10.1002/(SICI)1097-010X(19970801)278:5<299::AID-
830 JEZ4>3.0.CO;2-K
831 Kingsford MJ, Leis JM, Shanks A, et al (2002) Sensory environments, larval abilities and local
832 self-recruitment. Bull Mar Sci 70:309–340
833 Lau SCK, Mak KKW, Chen F, Qian PY (2002) Bioactivity of bacterial strains isolated from marine
834 biofilms in Hong Kong waters for the induction of larval settlement in the marine
835 polychaete Hydroides elegans. Mar Ecol Prog Ser 226:301–310.
836 https://doi.org/10.3354/meps226301
837 Lau SCK, Thiyagarajan V, Cheung SCK, Qian PY (2005) Roles of bacterial community composition
838 in biofilms as a mediator for larval settlement of three marine invertebrates. Aquat Microb
839 Ecol 38:41–51. https://doi.org/10.3354/ame038041
840 Lee JW, Nam JH, Kim YH, et al (2008) Bacterial communities in the initial stage of marine biofilm
841 formation on artificial surfaces. J Microbiol 46:174–182. https://doi.org/10.1007/s12275-
842 008-0032-3
843 Lee OO, Chung HC, Yang J, et al (2014) Molecular Techniques Revealed Highly Diverse Microbial
844 Communities in Natural Marine Biofilms on Polystyrene Dishes for Invertebrate Larval
845 Settlement. Microb Ecol 68:81–93. https://doi.org/10.1007/s00248-013-0348-3
846 Liberzon A, Birger C, Thorvaldsdóttir H, et al (2015) The Molecular Signatures Database
847 Hallmark Gene Set Collection. Cell Syst 1:417–425.
848 https://doi.org/10.1016/j.cels.2015.12.004
849 Liberzon A, Subramanian A, Pinchback R, et al (2011) Molecular signatures database (MSigDB)
850 3.0. Bioinformatics 27:1739–1740. https://doi.org/10.1093/bioinformatics/btr260
851 Mackie GO (1966) Growth of the hydroid Tubularia in culture. In: The Cnidaria and their
852 Evolution. pp 397–412
853 MacManes MD (2018) The Oyster River Protocol: a multi-assembler and kmer approach for de
854 novo transcriptome assembly. PeerJ 6:e5428. https://doi.org/10.7717/peerj.5428
855 Mason BM, Cohen JH (2012) Long-Wavelength Photosensitivity in Coral planula larvae. Biol Bull
856 222:88–92. https://doi.org/10.1086/BBLv222n2p88
857 Matsushima K, Kiyomoto M, Hatta M (2010) Aboral localization of responsiveness to a

858 metamorphic neuropeptide in the planula larva of Acropora tenuis. Galaxea, J Coral Reef
859 Stud 12:77–81. https://doi.org/10.3755/galaxea.12.77
860 McLaughlin S (2017) Evidence that polycystins are involved in Hydra cnidocyte discharge.
861 Invertebr Neurosci 17:1–14. https://doi.org/10.1007/s10158-016-0194-3
862 Meredith MA, Stein BE (1983) Interactions among converging sensory inputs in the superior
863 colliculus. Science (80-) 221:389–391
864 Mohapatra N, Mukherjee A, Suriya Rao A, et al (2014) Comparison of Different Parameters for
865 Evaluation of Partial Resistance to Rice Blast Disease. Am J Exp Agric 4:58–79.
866 https://doi.org/10.9734/ajea/2014/3756
867 Müller WA, Leitz T (2002) Metamorphosis in the Cnidaria. Can J Zool 80:1755–1771.
868 https://doi.org/10.1139/z02-130
869 Nellis P, Bourget E (1996) Influence of physical and chemical factors on settlement and
870 recruitment of the hydroid Tubularia larynx. Mar Ecol Prog Ser 140:123–139.
871 https://doi.org/10.3354/meps140123
872 Otto TU, Dassy B, Mamassian P (2013) Principles of multisensory behavior. J Neurosci 33:7463–
873 7474. https://doi.org/10.1523/JNEUROSCI.4678-12.2013
874 Patro R, Duggal G, Love MI, et al (2017) Salmon: fast and bias-aware quantification of transcript
875 expression using dual-phase inference. Nat Methods 14:417–419.
876 https://doi.org/10.1038/nmeth.4197.Salmon
877 Pawlik JR (1992) Chemical Ecology of the Settlement of Benthic Marine-Invertebrates.
878 Oceanogr. Mar. Biol. 30:273–335
879 Plachetzki DC, Fong CR, Oakley TH (2012a) Cnidocyte discharge is regulated by light and opsin-
880 mediated phototransduction. BMC Biol 10:. https://doi.org/10.1186/1741-7007-10-17
881 Plachetzki DC, Fong CR, Oakley TH (2012b) Cnidocyte discharge is regulated by light and opsin-
882 mediated phototransduction. BMC Biol 10:. https://doi.org/10.1186/1741-7007-10-17
883 Qian PY, Thiyagarajan V, Lau SCK, Cheung SCK (2003) Relationship between bacterial
884 community profile in biofilm and attachment of the acorn barnacle Balanus amphitrite.
885 Aquat Microb Ecol 33:225–237. https://doi.org/10.3354/ame033225
886 Rentzsch F, Layden M, Manuel M (2017) The cellular and molecular basis of cnidarian
887 neurogenesis. Wiley Interdiscip Rev Dev Biol 6:1–19. https://doi.org/10.1002/wdev.257
888 Say TE, Degnan SM (2020) Molecular and behavioural evidence that interdependent
889 photo - and chemosensory systems regulate larval settlement in a marine sponge. Mol
890 Ecol 29:247–261. https://doi.org/10.1111/mec.15318
891 Shaner G (1977) The Effect of Nitrogen Fertilization on the Expression of Slow-Mildewing
892 Resistance in Knox Wheat. Phytopathology 77:1051. https://doi.org/10.1094/phyto-67-
893 1051
894 Stein BE (1998) Neural mechanisms for synthesizing sensory information and producing
895 adaptive behaviors. Exp Brain Res 123:124–135. https://doi.org/10.1007/s002210050553
896 Stein BE, Meredith MA (1993) The merging of the senses. The MIT press
897 Stein BE, Meredith MA, Huneycutt WS, McDade L (1989) Behavioral indices of multisensory
898 integration: Orientation to visual cues is affected by auditory stimuli. J Cogn Neurosci
899 1:12–24. https://doi.org/10.1162/jocn.1989.1.1.12
900 Stein BE, Stanford TR (2008) Multisensory integration: Current issues from the perspective of
901 the single neuron. Nat Rev Neurosci 9:406. https://doi.org/10.1038/nrn2377

902 Stein BE, Stanford TR, Ramachandran R, et al (2009) Challenges in quantifying multisensory
903 integration: Alternative criteria, models, and inverse effectiveness. Exp Brain Res 198:113–
904 126. https://doi.org/10.1007/s00221-009-1880-8
905 Stein BE, Stanford TR, Rowland BA (2014) Development of multisensory integration from the
906 perspective of the individual neuron. Nat Rev Neurosci 15:520–535.
907 https://doi.org/10.1038/nrn3742
908 Stevenson RA, Ghose D, Fister JK, et al (2014) Identifying and Quantifying Multisensory
909 Integration: A Tutorial Review. Brain Topogr 27:707–730. https://doi.org/10.1007/s10548-
910 014-0365-7
911 Strader ME, Davies SW, Matz M V. (2015) Differential responses of coral larvae to the colour of
912 ambient light guide them to suitable settlement microhabitat. R Soc Open Sci 2:.
913 https://doi.org/10.1098/rsos.150358
914 Subramanian A, Tamayo P, Mootha VK, et al (2005) Gene set enrichment analysis: A knowledge-
915 based approach for interpreting genome-wide expression profiles. Proc Natl Acad Sci U S A
916 102:15545–15550. https://doi.org/10.1073/pnas.0506580102
917 Svane I, Dolmer P (1995) Perception of light at settlement: a comparative study of two
918 invertebrate larvae, a scyphozoan planula and a simple ascidian tadpole. J Exp Mar Bio Ecol
919 187:51–61. https://doi.org/10.1016/0022-0981(94)00171-9
920 Swafford AJM, Oakley TH (2018) Multimodal sensorimotor system in unicellular zoospores of a
921 fungus. J Exp Biol 221:. https://doi.org/10.1242/jeb.163196
922 Taddei-Ferretti C, Musio C, Santillo S, Cotugno A (2004) The photobiology of Hydra's periodic
923 activity. Hydrobiologia 530–531:129–134. https://doi.org/10.1007/s10750-004-2680-6
924 Tran C, Hadfield MG (2013) Localization of sensory mechanisms utilized by coral planulae to
925 detect settlement cues. Invertebr Biol 132:195–206. https://doi.org/10.1111/ivb.12025
926 Westfall JA (2004) Neural pathways and innervation of cnidocytes in tentacles of sea anemones.
927 Hydrobiologia 530–531:117–121. https://doi.org/10.1007/s10750-004-2678-0
928 Whalan S, Abdul Wahab MA, Sprungala S, et al (2015) Larval settlement: The role of surface
929 topography for sessile coral reef invertebrates. PLoS One 10:1–17.
930 https://doi.org/10.1371/journal.pone.0117675
931 Wieczorek SK, Todd CD (1998) Inhibition and facilitation of settlement of epifaunal marine
932 invertebrate larvae by microbial biofilm cues. Biofouling 12:81–118.
933 https://doi.org/10.1080/08927019809378348
934 Woodson CB, Webster DR, Weissburg MJ, Yen J (2007) Cue hierarchy and foraging in calanoid
935 copepods: Ecological implications of oceanographic structure. Mar Ecol Prog Ser 330:163–
936 177. https://doi.org/10.3354/meps330163
937 Yamashita K (2003) Larval Behavioral, Morphological Changes, and Nematocyte Dynamics
938 During Settlement of Actinulae of Tubularia mesembryanthemum, Allman 1871 (Hydrozoa:
939 Tubulariidae). Biol Bull 204:256–269
940 Zardus JD, Nedved BT, Huang Y, et al (2008) Microbial Biofilms Facilitate Adhesion in Biofouling
941 Invertebrates. Biol Bull 214:91–98. https://doi.org/10.2307/25066663
942
943